J. Fluid Mech. (1970), *vol.* 43, *part* 4, *pp.* 819–832
Printed in Great Britain

The flat plate boundary layer. Part 3. Comparison of theory with experiment

By J. A. ROSS, F. H. BARNES, J. G. BURNS AND M. A. S. ROSS

Fluid Mechanics Unit, Physics Department, University of Edinburgh

(Received 19 February 1970)

A study of Tollmien–Schlichting waves in the Blasius boundary layer has been carried out under good flow conditions. The maximum r.m.s. amplitude of u, the downstream component of perturbation velocity, was limited to about 0·06 % of U_0, the free-stream velocity. Measurements of the wave-number and of the distribution of u/U_0 normal to the plate agree closely with the theoretical results obtained in parts 1 and 2 of this paper. The experimental critical Reynolds number, R_c, is 400; the theoretical R_c derived from the imaginary part of the eigenvalue is 500 (part 2), but additional amplification carried by the eigenvector removes most of this discrepancy.

1. Introduction

In parts 1 and 2 of this paper an analysis by numerical methods has been given of the stability theory of the laminar boundary layer on a flat plate under zero pressure gradient. In this part these computed results will be compared with experiment.

The main evidence on the behaviour of two- and three-dimensional perturbations in the flat plate boundary layer has been obtained by Schubauer & Skramstad (1947), Schubauer & Klebanoff (1955) and Klebanoff, Tidstrom & Sargent (1962). The experiments to be reported here include repetitions of some of the two-dimensional work done by these authors at the National Bureau of Standards, Washington. The main difference between the present and previous work is that the predictions of theory are now more easily calculated for comparison with experiment.

2. The notation

In the following discussion, x represents downstream distance measured from the leading edge of the plate, z represents distance from the surface of the plate and t represents time. U and W symbolize the dimensional velocity components of the mean flow, u and w the dimensional velocity components of the perturbation and u' and w' the r.m.s. perturbation amplitudes. λ represents the wavelength and f the frequency of the perturbation.

In stability theory non-dimensional variables are used, and the non-dimensional stream function

$$\psi = \phi(Z)\, e^{i(\alpha X - \beta T)} \tag{1}$$

is substituted in the non-dimensional linearized vorticity equation for the perturbation to give the Orr–Sommerfeld equation for $\phi(Z)$. The equations are reduced to non-dimensional form by introducing U_0, the free-stream velocity, and δ_1, the displacement thickness of the boundary layer, in conjunction with ν, the kinematic viscosity. δ_1 is given by $m(\nu x/U_0)^{\frac{1}{2}}$, where $m = 1{\cdot}7208$. The non-dimensional variables are then: $R = U_0\delta_1/\nu$ (the boundary-layer Reynolds number), $X = x/\delta_1 = R/m^2$, $Z = z/\delta_1$, $T = U_0 t/\delta_1$ and $\beta = 2\pi f\delta_1/U_0 = FR$, where $F = 2\pi f\nu/U_0^2$ is known as the non-dimensional frequency parameter. In experimental work it is easier to keep F constant than to keep β constant, and the parameters R and F are therefore more convenient than R and β.

The solution of the Orr–Sommerfeld equation, as given in parts 1 and 2, involves the determination, for given real values of R and β, of a complex eigenvalue $\alpha = \alpha_r + i\alpha_i$, and a normalized complex eigenvector $\phi(Z) = \phi_r(Z) + i\phi_i(Z)$. To carry out a complete comparison of theory and experiment, four real quantities should therefore be measured for the given values of R and β, or R and F. In this paper, measurements of α_r and $|\phi'(Z)|$ will be reported first and the observed amplification will then be discussed. A study of the Reynolds stress, a suitable fourth observable, has not been made.

It is important to note that since the parameter α has been introduced through equation (1), it must be defined as a property of the stream function ψ. The reason why this is important is that measurements are of necessity made not on the stream function but on the perturbation velocity.

3. The real parts of the complex functions

The real part of the stream function ψ may be expressed as

$$\psi_r = Ce^{-\alpha_i X}|\phi(Z)| \cos(\alpha_r X - \beta T + \gamma) \tag{2}$$

and the corresponding form for the x component of the perturbation velocity is

$$u/U_0 = \partial\psi_r/\partial Z = Ce^{-\alpha_i X}|\phi'(Z)| \cos(\alpha_r X - \beta T + \kappa), \tag{3}$$

where

$$\phi_r(Z) = |\phi(Z)| \cos\gamma, \quad \phi_i(Z) = |\phi(Z)| \sin\gamma,$$
$$\phi_r'(Z) = |\phi'(Z)| \cos\kappa, \quad \phi_i'(Z) = |\phi'(Z)| \sin\kappa.$$

The computed values of the function $\phi(Z)$ are normalized by making $\phi_r(Z_n) = 1$ at the point Z_n where $\phi_r(Z)$ reaches its maximum value (see figure 5, part 1). The complete solution for $\phi(Z)$ must then include the amplitude factor C. We also have $\phi_r'(Z_n) = 0$ (see figure 6, part 1).

Since the computed values of α and $\phi(Z)$ are functions of R, each numerical integration gives a local solution; the dimensionless product $X\alpha_r = x(\alpha_r/\delta_1)$, and α_r/δ_1 is therefore the observable local wave-number $2\pi/\lambda$; the dimensionless product $-X\alpha_i = x(-\alpha_i/\delta_1)$, and $-\alpha_i/\delta_1$ is an observable local space rate of amplification. The r.m.s. velocity ratio is given by

$$\frac{u'}{U_0} = \left[\frac{\beta}{2\pi}\int_0^{2\pi/\beta}\left(\frac{u}{U_0}\right)^2 dT\right]^{\frac{1}{2}} = 2^{-\frac{1}{2}}Ce^{-\alpha_i X}|\phi'(Z)|. \tag{4}$$

Except in the immediate neighbourhood of the flat plate

$$\phi_i(Z) \ll \phi_r(Z), |\phi(Z)| \approx \phi_r(Z)$$

and except also close to Z_n, $\quad |\phi'(Z)| \approx \phi_r'(Z)$.

We also have

$$\int_0^{Z_n} \phi_r'(Z)\, dZ = \phi_r(Z_n) - \phi_r(0) = \phi_r(Z_n) = 1,$$

and an examination of the numerical solutions shows that

$$\int_0^{Z_n} |\phi'(Z)|\, dZ = I \approx 1$$

since I differs from unity by less than 1 %. Hence

$$\int_0^{Z_n} \left(\frac{u'}{U_0}\right) dZ = 2^{-\frac{1}{2}} C\, e^{-\alpha_i X}(1+\epsilon), \tag{5}$$

where ϵ is of the order of the fractional experimental error.

The total amplification of a disturbance propagating downstream at constant frequency is expressed (following Shen, private communication) as $\ln (A/A_0)$ where A is the amplitude of the disturbance at a point R and A_0, R_0 represent the amplitude and Reynolds number respectively at a point on branch I of the theoretical neutral stability curve having the given value of F (equation (5), part 1).

4. Experimental arrangements

The experiments were performed in a low-turbulence wind tunnel with a working section 10 ft. in length and 4 ft. × 4 ft. in cross-section. A flat plate, 9 ft. (2·74 m) long and 4 ft. (1·22 m) wide, of $\frac{1}{2}$ in. (12·7 mm) Perspex, with a symmetrically tapered leading edge, was installed in the central vertical plane. The section had a built-in slow expansion to reduce the pressure gradient, and had false walls for adjustment to zero pressure gradient. The distribution of pressure in the downstream direction measured at a wind speed of 40 ft./sec (12·2 m/sec) is shown in figure 1.

The boundary-layer perturbations were generated by a vibrating ribbon of phosphor-bronze strip, 0·1 in. in width and 0·001 in. in thickness. The ribbon was under adjustable tension and care was necessary to ensure that the tension on the two edges was equal. The vibrating length of the ribbon was limited by drawn glass bridges 0·0065 in. (0·165 mm) in diameter, mounted on the plate 4 in. above and 4 in. below the centre line. The ribbon was held firmly in contact with the bridges by applying sellotape strips about 1 in. above the upper bridge and 1 in. below the lower one to press the ribbon almost into contact with the plate. To avoid changes of tension a thin slip of paper was placed between the sellotape and the ribbon. A permanent magnet was mounted on the reverse side of the plate to produce a magnetic field in the x direction acting symmetrically on the ribbon. An a.c. current of frequency f, free from harmonic content within the limits of measurement (0·1 %), was passed through the ribbon, and if $\frac{1}{3}f_0 < f < \frac{2}{3}f_0$, where f_0 is the ribbon resonance frequency, the amplitude of ribbon

vibration was stable and proportional to the current, up to the point where it made contact with the plate (Kersley 1965).

The wind tunnel had a contraction ratio of 15 to 1, and the acoustic noise background was low. The total turbulence level $[\frac{1}{3}(u'^2+v'^2+w'^2)/U_0^2]^{\frac{1}{2}}$ measured in the frequency band 2 c/s to 20 kc/s, was of the order of 0·03 % in the working range of wind speeds. A study of the noise spectrum by Barnes (1966) showed that

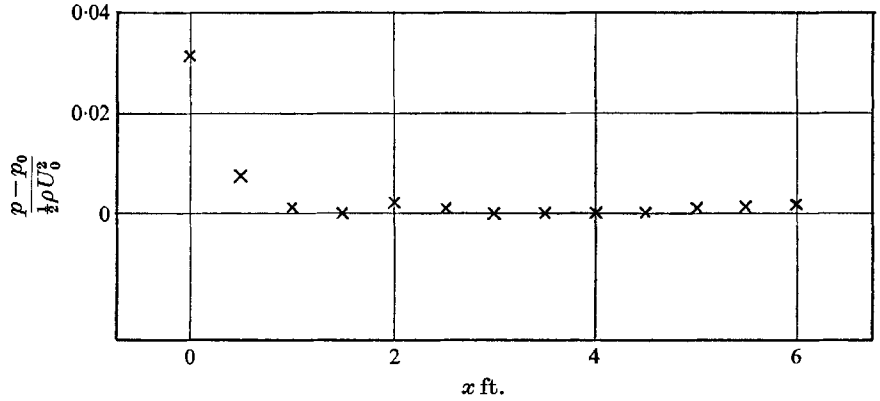

FIGURE 1. Variation of pressure in the working section of the tunnel as a function of x, the distance from the leading edge of the plate. p_0 = pressure measured at x = 3 ft. U_0 = 40 ft./sec.

about 98 % of this noise occurred at frequencies below those normally used for injected perturbations.

Measurements of velocity were made with a constant-current hot-wire anemometer made from Wollaston wire. The silver coating of the wire was removed with a fine jet of dilute nitric acid to expose about 1 mm length of the platinum core which had a diameter of 2×10^{-4} in. (5 μm). The d.c. voltage across the wire was measured directly. The a.c. voltage was passed to a low-noise preamplifier feeding a Bruel and Kjaer Frequency Analyser (Type 2107) with its r.m.s. output coupled to a Level Recorder. The ratio of signal to noise was maximized by using the most selective analyser band-width (6 % of mid-band frequency). With this arrangement, values of u'/U_0 of 0·02 % could be measured with an accuracy of about 2 %.

The calibration of the hot wire was carried out with a standard N.P.L. type Pitot-static tube and Chattock manometer. Since the Reynolds number of the wire in the free stream did not normally exceed 40, the calibration equation was taken in accordance with Collis & Williams (1959) to be

$$\sigma = r/(r-r_a) = A+BU^{0\cdot45},$$

where r and r_a represent the resistance of the wire at working and air temperatures respectively, and A and B are constants which are determined by least squares analysis of the calibration data.

The experimental measurements were made by carrying out traverses of the boundary layer, either at right angles to the plate (at constant x and varying z)

or downstream (at varying x). In a downstream traverse each setting generally involves adjustment of both x and z co-ordinates because small departures from flatness occur on the plate and small variations in z may be introduced by the x-traversing mechanism, both sources of variation being of the order of a few parts per cent of the boundary-layer thickness. Frequent determination of the zero of z is inconvenient, and in x traverses the anemometer was adjusted for 'constant resistance in the absence of injected perturbations'. This means that $(U^2+W^2)^{\frac{1}{2}}$ is kept constant, but since W is always less than $U/R_x^{\frac{1}{2}}$, the constant resistance condition means that U and hence z/δ_1 is kept constant. Provided it is clearly defined, the rule which is followed for the z position of the anemometer in x traverses is unimportant when traverses are made in both z and downstream directions, since the two sets of observations provide a complete map of the velocities within the layer.

5. Measurements of α_r

In this experiment measurements of the wavelength, λ, of a perturbation were made at constant U_0 and F by the Lissajous figure method, using a C.R.O. display. The X plates of the oscillograph were fed with a tapping from the ribbon current supply and the Y plates with the a.c. signal from the hot wire. The anemometer was traversed downstream for a total distance of about 4 ft., and readings of x were made after each complete wavelength. The initial amplitude of the perturbation was adjusted so that, after amplification in the boundary layer, the amplitude would satisfy the requirements of linearized theory. The values of x were read to 0·01 in., but the error involved in the Lissajous figure setting produced a standard deviation of 2 or 3 % in single measurements of λ.

The wavelength measurements were converted to values of $2\pi\nu/\lambda U_0$ (or $\alpha_r/\bar{R}$), where $\bar{R}$ is the mean of the Reynolds numbers at the beginning and end of the wavelength. Measurements were made for four values of $F\times 10^6$, namely 48·5, 81·4, 116·6 and 158·9. The results are shown in figure 2 as points on a graph of $\alpha_r/\bar{R}$ *versus* $\bar{R}$ for constant F. The continuous lines in the figure represent values of α_r calculated in part 2 for a boundary layer of increasing thickness. The lines are drawn for the following values of $F\times 10^6$: 50, 80, 116·6 and 160. After taking account of the differences in F between the experimental points and the corresponding theoretical lines, the observed values of α_r are found to be slightly below the theoretical ones by from 1·4 to 3 %.

6. The z-distribution of u'/U_0

In this experiment measurements were made of u'/U_0 as a function of z/δ, where δ is the total thickness of the boundary layer. Sufficiently small amplitudes of u' were used to ensure that the conditions of linearized theory would be satisfied. Values of U_0 and f were chosen to give a pre-determined value of F, and traverses were made in the z direction at a series of values of R, with F remaining as far as possible constant. For a given value of F the lowest value of R represented a position near branch I of the neutral stability curve, and the highest value a posi-

tion downstream of branch II. Three different values of $F \times 10^6$ were used, the mean values being 82, 110 and 157. After the observations were completed, Jordinson's programme (as described in part 1) was run to give the theoretical functions $|\phi'(Z)|$ for each pair of values of F and R used experimentally. The

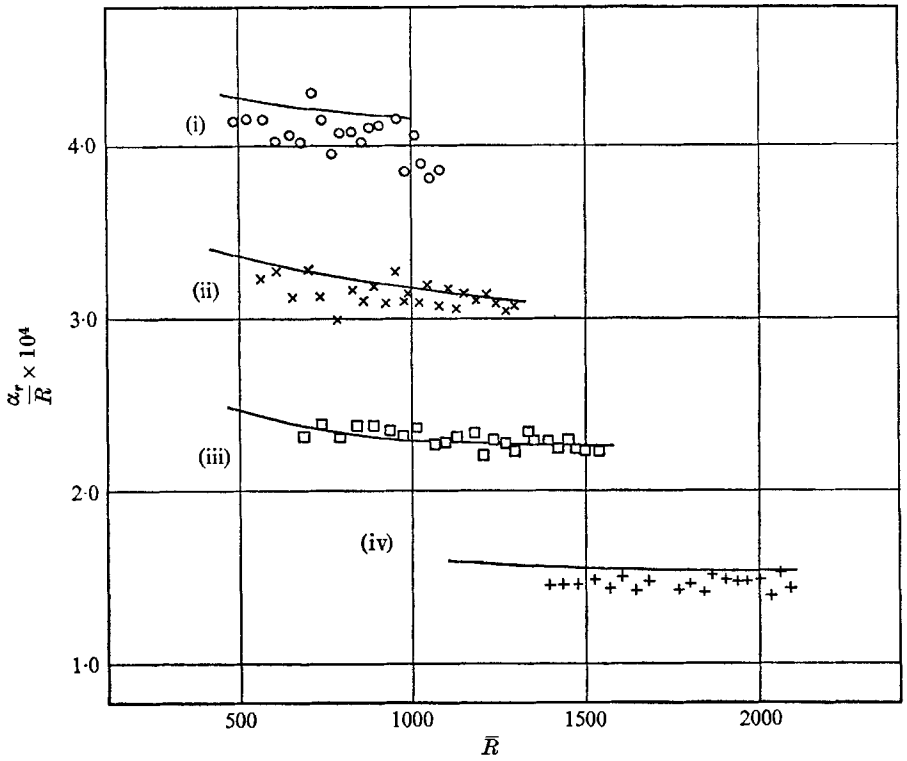

FIGURE 2. Comparison of theoretical and experimental values of $\alpha_r/\bar{R}$ as a function of $\bar{R}$ at constant F. Values of $F \times 10^6$:

	Theoretical line	Experimental points
(i)	160	158·9
(ii)	116·6	116·6
(iii)	80	81·4
(iv)	50	48·5

theoretical curves were normalized to the experimental ones by equalizing the areas under the two curves over the range $0 \leqslant z \leqslant \delta$, taking $\delta_1 = 0{\cdot}350\delta$. Figure 3 shows the experimental points and the theoretical curves for the six distributions of u'/U_0 obtained with $U_0 \approx 29$ ft./sec, $F \approx 82 \times 10^{-6}$ and Reynolds numbers of 770, 1073, 1212, 1363, 1396 and 1555. The scale on the vertical axes in this figure shows the percentage values of u'/U_0.

The shape of the theoretical curves for constant F shows a systematic variation as R increases, the minimum of the curve moving steadily inwards from about $z/\delta = 0{\cdot}785$ to about $z/\delta = 0{\cdot}635$, and the maximum moving from $z/\delta = 0{\cdot}25$ to

$z/\delta = 0{\cdot}10$. The complete set of experimental results (in figure 3 and all other traverses) shows no systematic departures from these features. Some allowance must be made for two sources of experimental error. (i) The hot-wire becomes

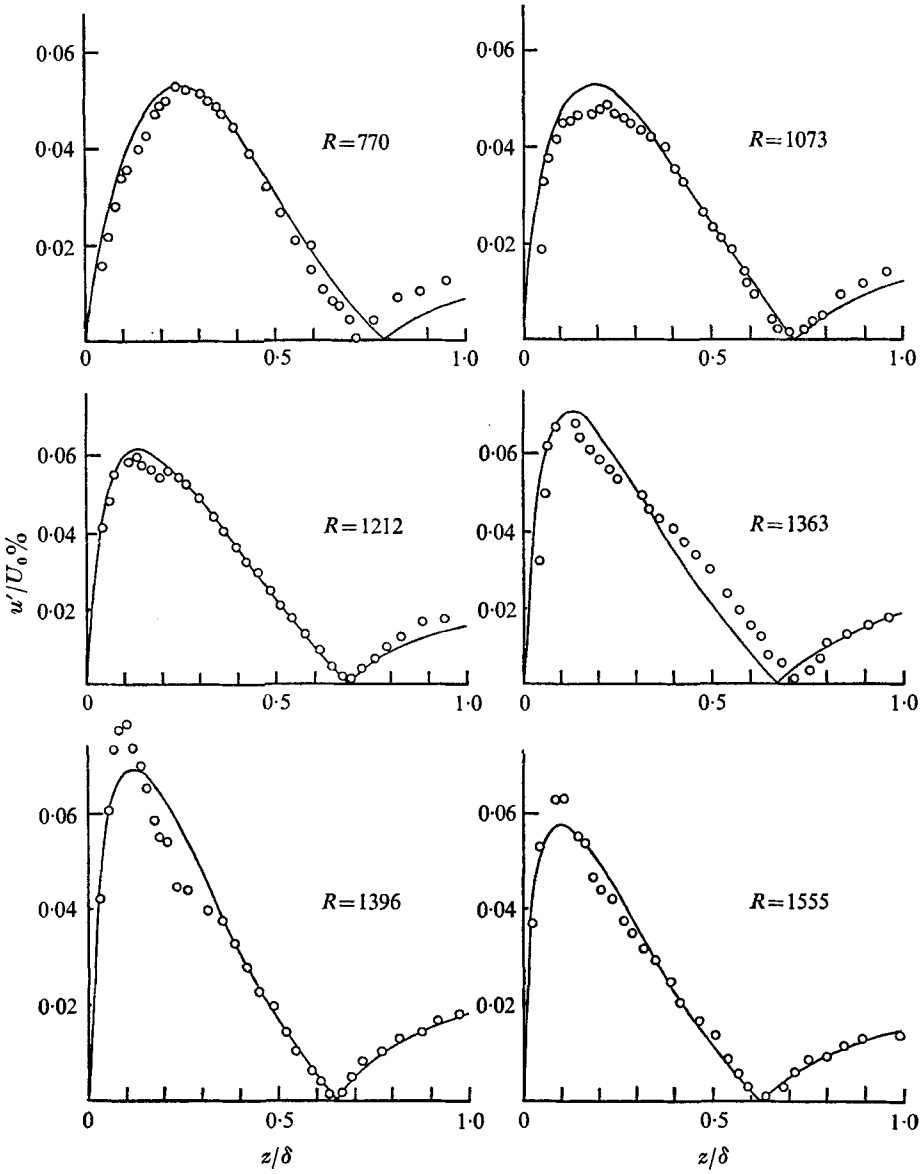

FIGURE 3. Comparison of theoretical curves of $|\phi'(Z)|$ and experimental values of u'/U_0 *versus* z/δ for $F = 82 \times 10^{-6}$ and various values of R.

more sensitive as z decreases and the wire temperature rises; the error involved in the wire calibration then becomes more important. (ii) Any instability in the support and control system of the instrument carriage, the boom and the clock gauge is liable to affect the measurements of z/δ. Evidence of the occurrence of

such errors can be seen in the observations, but the predicted shape of the distributions is, nevertheless, strongly confirmed by the experiments.

7. The neutral stability curve

Before the experiments reported above were carried out, measurements had been completed on the experimental neutral stability curve in the (F, R) plane, this curve being defined as the locus of $\partial u'/\partial x = 0$ for constant U_0 and F. Branches I and II of the curve are represented respectively by the minima and maxima of u'. Traverses in the x direction were first made to determine the branch II points. The hot wire was initially located at about $z/\delta = 0{\cdot}15$, and during the traverse its z position was controlled by adjusting for constant resistance in the absence of perturbations. Normally 12 or more successive readings were made at equal intervals of x, the total range of x being between 9 and 15 in. The maximum amplitude position was determined by fitting a cubic curve to the data by the least squares method, assuming that the error in x was negligible. It will be seen from figure 3 that in the neighbourhood of branch II, $z/\delta = 0{\cdot}15$ coincides quite well with the z-distribution maximum of u'/U_0, and no corrections were subsequently found to be necessary for the branch II points. In this series of observations the range $75 < F \times 10^6 < 250$ was studied. At higher F values the branch II points became more difficult to determine for reasons which will be discussed below.

When the experiments were continued to find points on branch I, the minima of u' were found to lie at unexpectedly low values of R by comparison with the calculated neutral stability curve. The ribbon was therefore moved upstream to a position 8 in. from the leading edge of the plate. No measurements were regarded as reliable within 2 in. of the ribbon, and the smallest value of x at which a minimum of amplitude could be established was 5 in. from the ribbon, or at least 13 in. from the leading edge of the plate. For Reynolds numbers between 370 and 500 we have $7 < U_0 x < 14$ in ft^2. sec^{-1}, and low values of U_0 were therefore required. U_0 was measured using the relation $\frac{1}{2}\rho U_0^2 = kd$, where d represents divisions on the Chattock scale and $2k/\rho \approx 1$. The reading error in d was about 4 divisions. Thus when U_0 was 10 ft./sec, $d \approx 100$ and the error in U_0^2 was 4 %. Hence the error in F was 4 % and the error in $R = (U_0 x/\nu)^{\frac{1}{2}}$ was 1 %. Trouble was also encountered when F lay in the range $150 < F \times 10^6 < 300$, for then $7 < U_0^2/f > 3{\cdot}5$ in ft^2. sec^{-1} and small values of f below 20 c/s were required when U_0 was small. The low frequency limit of the Frequency Analyser was 20 c/s, and when f lay below this limit, the signals had to be recorded on an E.M.I. frequency modulated tape recorder and played back for measurement at four times the recording tape speed. The limit of useful work was reached when the error in R rose to 2 % and the error in F to 8 %. No points on branch I were therefore observed for F values above 300×10^{-6}.

Finally, points on branch II with high F values were found. The highest F value at which amplification was definitely observed was $401{\cdot}3 \times 10^{-6}$, and the lowest F value showing continuous damping was about 430×10^{-6}.

In the subsequent studies of the z distribution of u'/U_0 (as shown in figure 3) and of the amplification curves (to be discussed below) it was found that a

systematic error of -20 units of R occurred in the determination of the branch I points. This arose through the use of $z/\delta = 0{\cdot}15$ for the initial location of the anemometer. A correction for this error has been applied to all the branch I points. The results of this work are shown in figure 4.

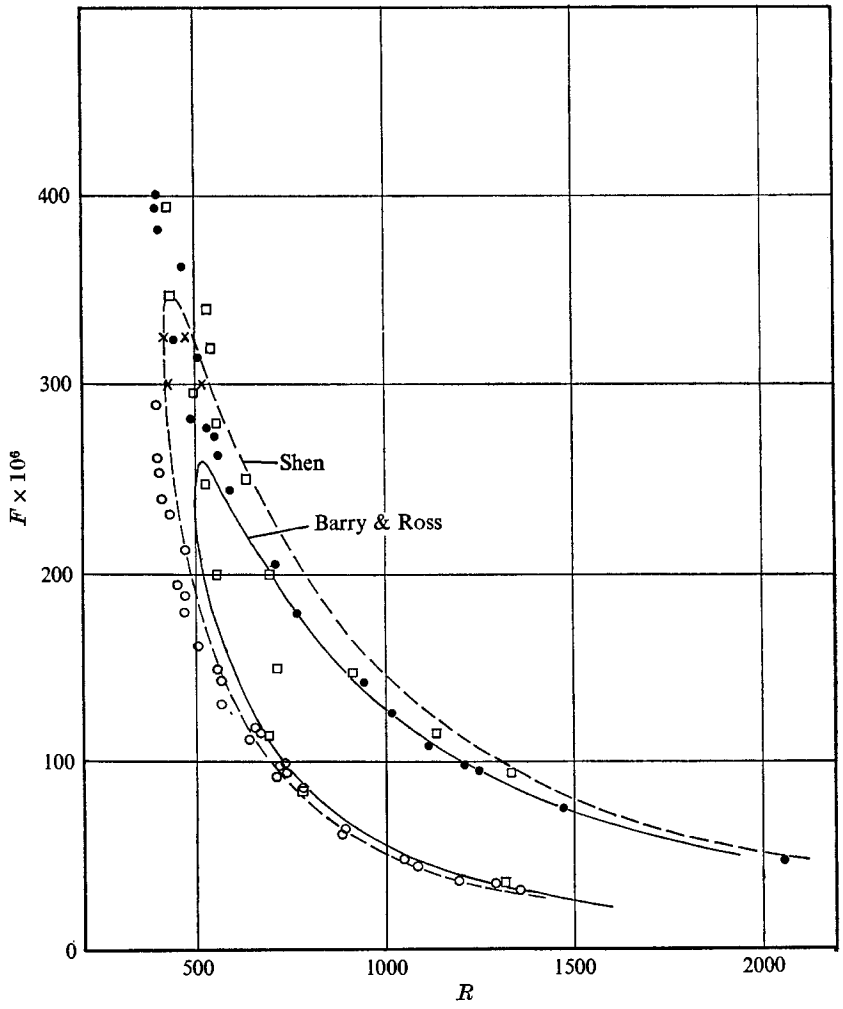

FIGURE 4. Comparison of neutral stability curves calculated by Shen (1954) and Barry & Ross (part 2) with experimental points. □, Schubauer & Skramstad (1947); ○, present results for branch I; ●, present results for branch II; ×, points computed by Barry for $\alpha_T = 0$.

8. The parameter α_i

In figure 5 a portion of the boundary layer is represented by a graph of z/δ *versus* R, with PP' representing the surface of the plate and QQ' the outer edge of the layer. QP and $Q'P'$ represent respectively branches I and II of the neutral stability curve for a perturbation of frequency parameter F. It is assumed that

a disturbance having this frequency parameter has entered the layer upstream of branch I. The lines *ABC* and *DEF* represent respectively the loci of the minimum and maximum in the z distribution of u'/U_0 at any R. Then to a good approximation

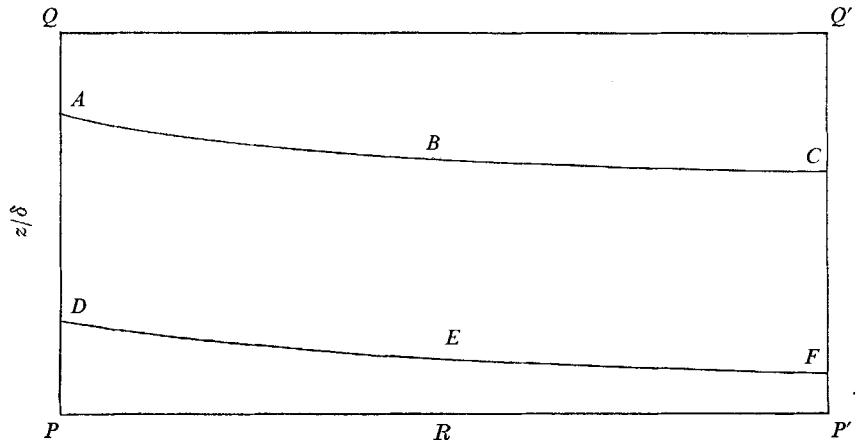

FIGURE 5. Diagram of the boundary layer; z/δ *versus* R. PP', the plate surface; QQ', the upper edge of the layer; PQ, branch I; $P'Q'$, branch II; ABC, locus of velocity minimum; DEF, locus of velocity maximum.

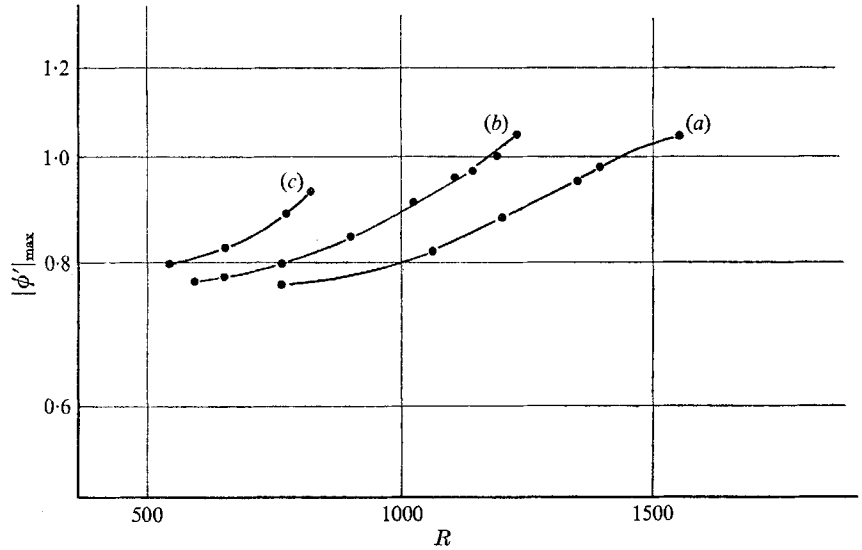

FIGURE 6. Amplification carried by the eigenvector for constant F and varying R. $|\phi'|_{\max}$ *versus* R. (*a*) $F = 82 \times 10^{-6}$, (*b*) $F = 110 \times 10^{-6}$, (*c*) $F = 157 \times 10^{-6}$.

ABC is the locus of Z_n. If measurements of the total amplification of the perturbation are required, the best procedure would appear to be to traverse the anemometer along the line DEF to obtain measurements of $(u'/U_0)_{\max}$.

From equation (4) the maximum value of u'/U_0 at a given value of X depends on the maximum value of the function $|\phi'(Z)|$. The numerical solutions for $|\phi'(Z)|$ which were obtained for comparison with experiment (see § 6 above) showed that, when F remains constant and R increases, the maximum value of $|\phi'(Z)|$ increases

steadily between branch I and branch II. Figure 6 shows a graph of $|\phi'|_{\max}$ as a function of R for the three values of F reported on in § 6. The observed amplification of u'/U_0 must include the increase in $|\phi'|$ as well as the increase from the exponential factor in equation (4). The variation in the peak value of $|\phi'|$ is, of course, associated with the normalization which was applied to $\phi_r(Z)$, making $\phi_r(Z_n) = 1$.

Taking logarithmic differentials with respect to X of $(u'/U_0)_{\max}$, we obtain from (4):

$$\frac{d}{dX}[\ln (u'/U_0)_{\max}] = -\alpha_i + \frac{d}{dX}[\ln \phi'(Z)_{\max}] = -\alpha_T, \tag{6}$$

where $-\alpha_T$ is the space rate of amplification of $(u'/U_0)_{\max}$ corresponding to $-\alpha_i$, the space rate of amplification of the flux.

If we wish to compare theoretical and experimental values of α_i it will be necessary either to use equation (5) or to obtain a succession of values of $(u'/U_0)_{\max}$ and correct the rate of amplification $-\alpha_T$ by equation (6) to obtain $-\alpha_i$. The local rates of amplification can be obtained only by differentiating the growth curves, and this is a process which cannot be performed with sufficient accuracy. It is therefore preferable to compare the calculated and observed growth curves expressed in terms of $\ln (A/A_0)$.

Three different methods were used to obtain data for comparison with the computed values of $\ln (A/A_0)$ as a function of R at constant F (part 1).

(i) The integral

$$\int_0^{Z_n} (u'/U_0)\, dZ$$

was evaluated from the z distributions. When the z distributions were obtained for a given F, different amplitudes of ribbon vibration were required at different values of R. The data were therefore reduced to a common ribbon amplitude.

(ii) The peak values of the same z distributions were read and were likewise reduced to common ribbon amplitude.

(iii) A series of traverses in the x direction were made at constant U_0 and at the same values of F. Four traverses were made for each F at values of z/δ of 0·125, 0·20, 0·30, and 0·415. A correction was then applied, using Jordinson's functions $|\phi'(Z)|$, to obtain the peak amplitudes along the line DEF.

The observed amplitudes for each F were then reduced to values of $\ln (A/A_0)$ and a correction for the $|\phi'|$ amplification was applied to the data obtained by methods (ii) and (iii). This correction produced only a small downstream shift of the branch I point in the case of the two lower frequencies ($F = 82 \times 10^{-6}$ and $F = 110 \times 10^{-6}$) but moved branch I downstream by 40 units of R for $F = 157 \times 10^{-6}$. These shifts of R were such as to bring the branch I points into quite good agreement with the theoretical neutral stability curve $\alpha_i = 0$ (part 2, figure 1).

The three sets of values of $\ln (A/A_0)$ showed no systematic differences associated with the method of measurement, and mean values were taken. These are compared in figure 7 with the theoretical curves interpolated from the results obtained in part 1. If the theoretical curves in this figure had been obtained for a boundary layer of growing thickness the height of these curves would have been

about 9 % higher at $F \times 10^6 = 82$, about 11 % higher for $F \times 10^6 = 110$, and between 15 and 20 % higher at $F \times 10^6 = 157$. When account is taken of the possibility of spanwise energy transfer, the agreement between theory and experiment seems reasonable although not close.

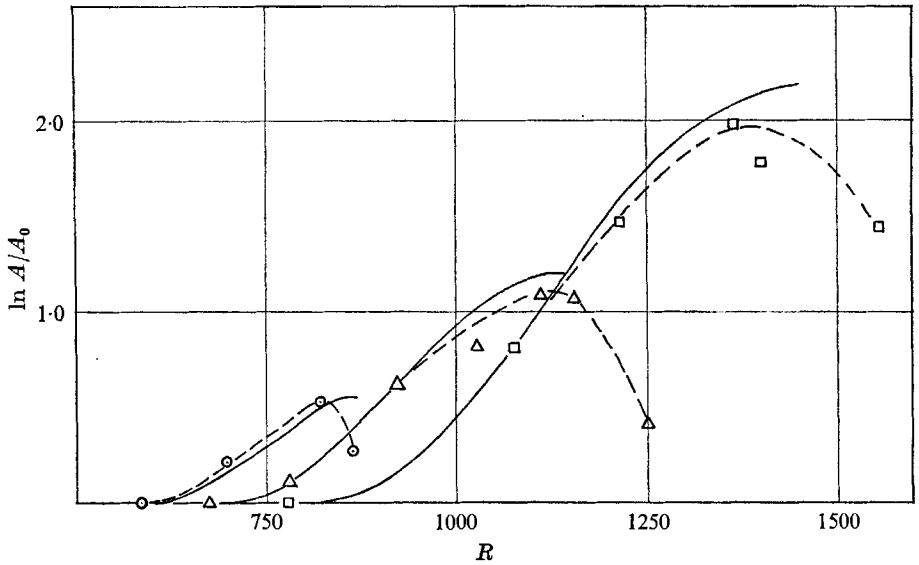

FIGURE 7. Amplification contributed by α_i; curves for constant F and varying R. ———, theoretical results of Jordinson (part 1); – – – –, approximate experimental curves. □, $F = 82 \times 10^{-6}$; △, $F = 110 \times 10^{-6}$; ⊙, $F = 157 \times 10^{-6}$.

As a further test of our method of reconciling the experimental neutral stability curve with theory, calculations were carried out to find some points on the curve of $\alpha_T = 0$ in the (F, R) plane. In these calculations α_i and $|\phi'(Z)|$ were found for a series of equally spaced values of R at constant F. Then using equation (6), α_T was obtained for a number of consecutive values of R, and by interpolation the values of R for $\alpha_T = 0$ were found. These calculations were first performed by Jordinson, using a programme which included the 'parallel mean flow' assumption. They were later repeated by Barry using the programme for a boundary layer of growing thickness. The results are shown in the following table:

Points with $\alpha_T = 0$ in the (F, R) plane

Author	$F \times 10^6$	R Branch I	R Branch II	Computing interval ΔR
Jordinson	80	810	—	100
	160	565	—	100
	300	442	506	50
Barry	300	430	520	50
	325	424	477	50
	350	$\alpha_T \approx 0$ but positive		50

The four points found by Barry, two on branch I and two on branch II, are shown as crosses in figure 4. A comparison of the two sets of results at $F \times 10^6 = 300$ shows that the growth of boundary-layer thickness is a destabilizing influence, even at high F values.

The error in these calculations is estimated to be of the order of 5 units of R in the frequency region $F \times 10^6 = 300$ and greater, and at the lower frequencies is about 2 units of R. The most interesting feature of the results is the fairly close agreement between our calculated points and the neutral stability curve calculated by Shen (1954) following the method of Lin (1945). The critical Reynolds number on Shen's graph is about 423, and the highest value of F which is reached is about 346×10^{-6}.

9. General interpretation

The results of the experiments reported in §§ 5 and 6 on α_r and the z distribution of u'/U_0 are in close agreement with the corresponding theoretical results obtained by numerical analysis of the Orr–Sommerfeld equation for the space amplification case. The systematic difference between calculated and experimental values of α_r is reduced from about 4 % to about 2 % when the calculations in part 2 are used in place of those in part 1.

The study of boundary-layer amplification in §§ 7 and 8 has, however, revealed a more complicated situation. The experimental neutral stability curve, based on the minima and maxima of u' in downstream traverses, is not in agreement with the theoretical curve for $\alpha_i = 0$ in the (F, R) plane. The minimum critical Reynolds number found in experiments is about 400, while the part 1 calculations give 520 and the part 2 calculations give 500. The experimental maximum F value is about 400×10^{-6} and the calculated values are about 245×10^{-6} (part 1) and 260×10^{-6} (part 2). Thus at low Reynolds numbers and high F values the boundary layer is considerably less stable than the calculations indicate on the basis of the locus of $\alpha_i = 0$.

This problem has been largely resolved by examining the calculated values of the function $|\phi'(Z)|$ which occurs in the theoretical expression for the r.m.s. velocity ratio u'/U_0. The integral of this function between the limits 0 and Z_n is approximately constant, while the distance between the plate and Z_n decreases and the peak value of $|\phi'(Z)|$ increases as R increases. This property of the solution given in part 1 has been easy to interpret on account of the normalization procedure which has been applied to $\phi_r(Z)$. The discrepancy between the experimental neutral stability curve and the curve $\alpha_i = 0$ has been reduced from 100 units of R to about 25 units by taking account of the amplification included in $|\phi'|_{\max}$ and using calculated values of $\alpha_T = 0$ as the theoretical curve.

It should, nevertheless, be noted that the original linearized vorticity equation for the perturbation:

$$\frac{\partial}{\partial T}\nabla^2\psi + U\frac{\partial}{\partial X}\nabla^2\psi + W\frac{\partial}{\partial Z}\nabla^2\psi + \frac{\partial\psi}{\partial Z}\cdot\frac{\partial H}{\partial X} - \frac{\partial\psi}{\partial X}\cdot\frac{\partial H}{\partial Z} = \frac{1}{R}\nabla^4\psi, \tag{7}$$

where

$$H = \partial U/\partial Z - \partial W/\partial X,$$

is separable in time but not in X and Z. The failure to separate results from the presence of the terms

$$U\frac{\partial^3\psi}{\partial X\,\partial Z^2}, \quad W\frac{\partial^3\psi}{\partial X^2\,\partial Z} \quad \text{and} \quad \frac{1}{R}\frac{\partial^4\psi}{\partial X^2\,\partial Z^2},$$

the first of these terms being the most important. In order to reduce (7) to an ordinary differential equation in Z, a separable form of stream function such as (1) must be used. The function $\phi(Z)$ and the eigenvalue α may then be found for various values of R and β. $\phi(Z)$ shows only a small dependence on R, but since $R = Xm^2$, the function ϕ carries a weak X dependence which has necessarily been ignored in deriving the Orr–Sommerfeld equation.

The parameter α_r and the function $|\phi'(Z)|$ are found experimentally to be only slightly dependent on R, and this may explain the good agreement between theory and experiment for these functions. But α_i is strongly R dependent, and it is therefore possible that larger errors occur in the calculated values of this function. If this is the case, then any errors in α_i can be compensated within the limits of present theory only by allowing the constant C to become R dependent.

A conclusive way of dealing with the amplification would be to substitute the stream function in the form

$$\psi = f(X, Z)\, e^{-i\beta T}$$

and integrate the resulting partial differential equation with respect to both X and Z. The obstacle to this procedure is the absence of appropriate boundary conditions at two different values of X. It is possible, however, that a sufficiently accurate set of boundary conditions could be provided by experiment. In order to obtain valid boundary conditions for X, stringently two-dimensional experimental conditions would be needed.

The work reported above has been made possible by the award of the following grants which are gratefully acknowledged. Grants to cover the cost of construction of the low-turbulence wind tunnel and provision of a PDP-8 Computer were made by the Science Research Council. A maintenance grant for one of the authors (J.A.R.), the salary of a technician, and substantial support for the wind tunnel instrumentation were received from the Ministry of Technology.

REFERENCES

Barnes, F. H. 1966 Ph.D. thesis. Edinburgh University.

Collis, D. C. & Williams, M. J. 1959 *J. Fluid Mech.* **6**, 357.

Kersley, L. 1965 Ph.D. Thesis, Edinburgh University.

Klebanoff, P. S., Tidstrom, K. D. & Sargent, L. M. 1962 *J. Fluid Mech.* **12**, 1.

Lin, C. C. 1945 *Quart. J. Mech. Appl. Math.* **3**, 277.

Schubauer, G. B. & Skramstad, H. K. 1947 *J. Res. Nat. Bur. Stand.* **38**, 251.

Schubauer, G. B. & Klebanoff, P. S. 1955 *Nat. Advis. Comm. Aero. Wash. Rep.* no. 1289.

Shen, S. F. 1954 *J. Aero. Sci.* **21**, 62.